Eur. Phys. J. B **48**, 367–372 (2005)
DOI: 10.1140/epjb/e2005-00407-9

THE EUROPEAN PHYSICAL JOURNAL B

Effects of Gd^{3+} doping on structural and dielectric properties of PZT (Zr:Ti = 52:48) piezoceramics

L. Pdungsap[1], S. Boonyeun[2], P. Winotai[1], N. Udomkan[3,a], and P. Limsuwan[4]

[1] Department of Chemistry, Faculty of Science, Mahidol University, Rama VI Road, Bangkok 10400, Thailand
[2] Department of Chemistry, Faculty of Science, Thammasat University, Phaholyothin Road, Bangkok, Thailand
[3] 846/227 Bangmod, Prachautid 44, Thungkru, Bangkok 10140, Thailand
[4] Department of Physics, Faculty of Science, King Mongkut's University of Technology, Thonburi, Bangkok 10140, Thailand

Received 16 May 2005
Published online 23 December 2005 –

Abstract. The purpose of this research is to study the effect of doping Gd into $Pb(Zr_{0.52}Ti_{0.48})O_3$ ceramics prepared by solid state reaction. X-ray diffraction patterns show that all PGZT samples are of tetragonal structure and the highest doping should be no more than 2 mole % Gd at which the unreacted oxides start to appear. The electron spin resonance (ESR) spectra of PGZT's indicate that Gd^{3+} can enter both A site of the perovskite structure instead of only A site as widely believed. The ESR peaks resonance shift towards low fields as the concentration is higher, which is due to the change in crystal field experienced by Gd^{3+} ions. At $x = 0.001$, 0.005 and 0.01 dopings, two sets of powder ESR signals arising from Gd^{3+} ($4f^7$, spin 7/2) ions at A site. The first set shows some fine structure having strong absorption peaks centered at 76.26 mT ($g = 8.550$). The second is a seven-peak spectrum centered at 206.01 mT ($g = 3.165$), which belongs to the Gd^{3+} ions at B sites. Furthermore, the overlapped ESR strong absorption peaks from 309.17 mT to 314.49 mT ($g = 2.2818-2.1087$) belong to Gd^{3+} of unreacted Gd_2O_3. The local environments of Gd^{3+} ions were verified from the calculated ESR spectra using appropriate spin Hamiltonian parameter, i.e. gyromagnetic tensor **g**, zero-field splitting $\boldsymbol{D}$ and hyperfine tensor $\boldsymbol{A}$.

PACS. 61.10.Nz X-ray diffraction – 76.30.kg Rare-earth ions and impurities – 77.65.-j Piezoelectricity and electromechanical effects

1 Introduction

Since early 1970's, $Pb(Zr_{1-x}Ti_x)O_3$ (the so-called PZT) a solid solution between $PbZrO_3$ and $PbTiO_3$ has been known to exhibit a morphotropic phase boundary (MPB) separating a tetragonal ferroelectric phase with $x > 0.52$ from a rhombohedral ferroelectric phase with $0.06 < x < 0.45$ [1]. At $x \leq 0.06$ the compositions form an orthorhombic antiferroelectric phase. However, by using synchrotron X-ray powder diffraction, researchers have recently discovered a new phase with $0.45 < x < 0.52$ which is monoclinic ferroelectric at low temperature [2]. A key feature of the new structure is that the polarization vector is no longer constrained to point along a symmetry axis, as in the rhombohedral (R) and tetragonal (T) structures, but can rotate within the monoclinic plane [3–5]. The PZT piezoelectric ceramics have a wide range of applications due to their large electromechanical conversion efficiency. At room temperature, the c/a ratio of $Pb(Zr_{0.5}Ti_{0.5})O_3$ [the so-called PZT (50:50)] is 1.029 and the mechanical quality factor (Q_m) is 200 and the Curie temperature is at 380 °C. However, in the vicinity of MPB, $Pb(Zr_{0.48}Ti_{0.52})O_3$[i.e. PZT(48:52)] has a Q_m value of 500 which is more than twice the value of PZT (50:50), and with a slightly higher T_c of 386 °C. In order improve the properties of the ceramics for particular applications, impurities have been added to the PZT. The isovalent substitution of Sr^{2+} to the Pb^{2+} site [6] lowers T_c approximately by 9.5° per atom percent added and raises the dielectric constant at room temperature. Since the coupling factor and elastic modulus are not changed considerably, this results in higher value piezoelectric constant (d_{33}). Furthermore, the dissipation factor remains quite low and the electromechanical coupling in the vicinity of the MPB seems to be a little higher. Comparing to the unmodified, $Pb_{0.94}Sr_{0.06}(Zr_{0.53}Ti_{0.47})O_3$ is somewhat more difficult to depose by electrical or mechanical means. Additives doped into B site can be classified as being "donor type" or "acceptor type". The former type (Nb^{5+} and Ta^{5+}) leads to a higher electromechanical coupling factor (k_{13}) and a lower Q_m while the latter (Fe^{3+}, Mg^{2+} and Al^{3+}) lowers the k_{13} but increase Q_m. Manganese dose not belong to either of them. Doping Mn into PZT [7] increase the Q_m in a parabolic manner, the increase being greater with sintering done in nitrogen atmosphere than in air. However, sintering in oxygen lowers the

[a] e-mail: nitinai_udomkan@yahoo.com

Q_m. The addition of Mn under all atmosphere and heating conditions increased the electro-mechanical coupling factor. Increasing the ratio of Mn^{2+}/Mn^{3+} doping lowers T_c and tetragonality or, in other words the c/a ratio. The reduction of tetragonality leads to the lower saturation polarizations. According to Takahashi and Hirose [8], the effects of different types of additive on the values of Q_m is due to fact that donor dopant makes it easy for the ferroelectric domain to move, while the acceptor dopant makes it more difficult for the domain walls to move. Since the hysteresis loss due to the wall movement decreases the Q_m values, the effect of the dopant is compensated by a round about manner. In the Nb-modified PZT, $Pb_{1-x/2}(Zr_{0.52}Ti_{0.48})_{1-x}Nb_xO_3$ which is close to the MPB, T_c is lowered from 382 °C for $x = 0.000$ to 365 °C for $x = 0.024$ with the increase in Nb. Many metallic ions can be incorporated into A site of the PZT lattice. The group of ions of particular interest is of lanthanide series, which may easily find applications in pyroelectric [9], electro-optic [10] and infrared devices [11].

The piezoelectric materials are commonly found in commercial sensors and actuators. These materials can convert electrical energy into mechanical energy or vice versa [12,13]. The brief description of various piezoelectric materials with compositional families will be mentioned that are arranged with respect to transition temperature. More emphasis will be given on the high transition temperature (T_c) of the materials. In 1990, Kim et al. [14] reported Q_m and planer coupling coefficient (k_p) of $Pb(Zr_{0.52}Ti_{0.48})O_3$ could be improved by adding small amount of MnO_2. Kamiya et al. [15] studied further in 1992 the effects of manganese addition on piezoelectric properties of Pb $(Zr_{0.5}Ti_{0.5})O_3$ which they reported that MnO_2 addition increased Q_m and k_{31} at low poling field. These results indicated that Mn-doped PZT possessed properties of 'hard' piezoelectric simultaneously. Electron spin resonance (ESR) measurements showed that Mn^{2+}, Mn^{3+} and Mn^{4+} could coexist in PZT. Furthermore, the tetragonality of the PZT system and its Curie temperature decreased with MnO_2 content. These results led to the conclusion that the increase in k_{31} of Mn-doped PZT was due to the change of the crystal structure toward a cubic system, and the increase in Q_m to Mn^{2+} and Mn^{3+} ions working as acceptor dopants. The substitution of Cr^{+3}, Fe^{3+} and Mn^{3+} into Ti^{4+} sites, which are well known as 'acceptor-type' ions, associate with the O^{2-} vacancies which increase the Q_m by suppressing domain wall motions in response to applied electric field, observed by Hayashi et al. in 1998 [16]. They studied the effect of Mn ions in PT ceramics by means of ESR, which is one of the most useful techniques used to identify the valence states and lattice sites for the doping ions. Hayashi et al. also indicated that Mn ions associated with oxygen vacancies due to the substitution at the Ti^{4+} site, are incorporated as acceptor ions such as Mn^{2+} or Mn^{3+} to increase Q_m. For high-power piezoelectric actuator devices such as ultrasonic motors and piezoelectric transformers, it is necessary to have a high Q_m and low dielectric loss (tan δ). In 1999, Kim and co-workers [17] studied the effect of Fe_2O_3 doped $0.57Pb(Sc_{1/2}Nb_{1/2})O_3$-$0.43PbTiO_3$ ceramic materials. They reported that the Q_m increased by addition of acceptor dopants of Fe_2O_3, while dielectric loss tended to decrease. In 1999, Galassi and co-workers [18] reported that certain PZT ceramics doped with Nb, Mg, Mn and Li under optimized conditions possessed very high Q_m and k_p together with small dielectric loss. Such ceramics could be considered as hard ferroelectric ceramics. The properties of gadolinium modified PZT ceramics have been investigated in the present work to understand the effects of gadolinium ions on their structural, dielectric and piezoelectric properties. Since the dopant may be have drastic effects on the piezoelectric properties of PZT ceramics, it is not yet clear whether the dopant enters A or B site, especially for the Gd^{3+} ion. We want to investigate this by using ESR spectrometer to check whether the ions enter both sites as has been earlier proposed [19]. Gd^{3+} is chosen because of its rather long spin lattice relaxation time so that the ESR signal can be detected easily at room temperature as well as at liquid nitrogen temperature.

2 Experimental procedures

Gadolinium-doped lead zirconate titanate (PGZT) ceramics samples having different Gd^{3+} concentrations were prepared from high purity metal oxides via conventional mixed oxide method. The oxide powders were weighed in stoichiometric proportion and then mixed to obtain $Pb[Gd_x(Zr_{0.52}Ti_{0.48})_{1-x}]O_3$ for Gd^{3+} (PGZT) where $x =$ 0.0001, 0.001, 0.005, 0.01, 0.02, 0.06 and 0.10 respectively. The formulation was based on the assumption that Gd^{3+} would substitute Zr^{4+}/Ti^{4+} on B site. All oxides, except PbO, were first heated to eliminate moisture and existing organic impurities at 800 °C for 2 h. PbO was heated at 600 °C due to its volatility. The stoichiometric mixtures were homogenized in ethanol for 24 h. The resulting mixtures were dried at 100 °C, ground and calcined at 800 °C for 2 h. The products were reground to fine powder and sieved though a 75-micron sieve. The X-ray diffractometer (CuK_α) was used to check for PGZT phase before pressing the powder into pellets with 2wt % PVA binder added, under 2000 psi pressure and further subjected to a cold isostatic press at 28 000 psi. They were then put in a closed alumina crucible and separated by thin layers of $PbZrO_3$ powder to prevent them from fusing during the one-hour 1200 °C sintering. During the process, extra amount of PbO_2 was added to compensate for loss of PbO. The density of sintered pellets was measured while the structures of PGZT ceramics were again checked by X-ray diffractometer. To measure the dielectric constants and the piezoelectric properties, the pellets were sliced into thin discs of one mm thick. They were then poled for 30 minutes at 30 KV/cm in 100 °C silicone oil bath. Meanwhile, PGZT powders of about 30−60 mg were required to measure ESR spectra in X-band (TE_{011} mode) JEOL JES-RE2X spectrometer using 0.5 mT field (100 kHz) modulation. All ESR experiments were carried out both at room and liquid nitrogen temperature (295 K and 77 K). Each PGZT sample was accurately weighed

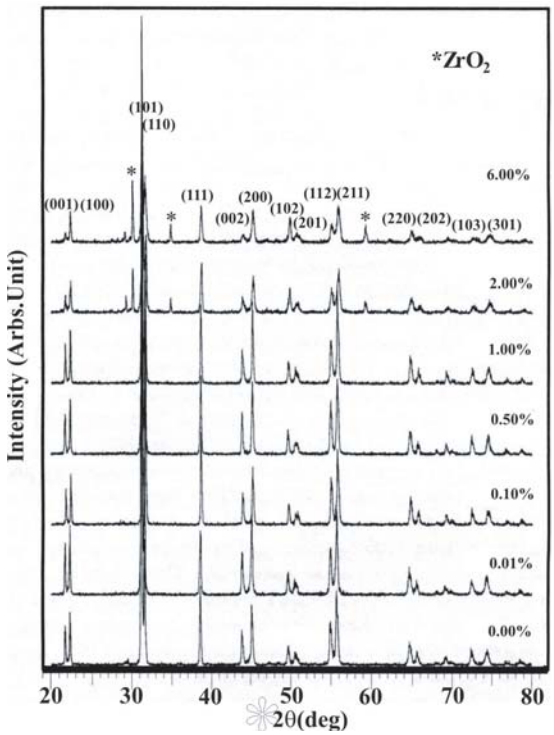

Fig. 1. X-ray diffraction patterns of PGZT having different mole percents of Gd^{3+} dopings.

before putting in a clean sample tube so that the intensity of Gd^{3+} ESR signals in the PZT structure and those from impurity phases could be compared.

3 Results and discussions

3.1 X-ray diffractograms

Powder X-ray diffraction patterns of PGZT samples at various Gd^{3+} dopings are shown in Figure 1. It is clearly evident from well-resolved peaks of the (002) and (200) planes that the ceramics are of tetragonal phase. A few peaks belonging to traces of unreacted ZrO_2 and Gd_2O_3 start to appear at 2% Gd^{3+} doping. By doing a Rietveld refinement of the XRD peaks, two of which are displayed in Figure 2, the lattice parameters a and c can be obtained and the tetragonality (c/a ratio) as a function of Gd^{3+} concentrations in PGZT is shown in Table 1. It can be seen that doping by Gd^{3+} leads to an increase in the ratio of c/a for low Gd^{3+} concentrations until it reaches a maximum where x is approximately equals to 0.01. The ratio then decreases sharply for $x > 0.01$ which clearly indicates Gd^{3+} first enters B site and then A site at higher concentrations. This results from the fact that the ionic radius of Gd^{3+} (0.94 Å for coordination number = 6) [20] is much smaller than that of Pb^{2+} (1.19 Å). It is widely believed that the excess positive charge is compensated by the creation of vacancies at B sites. However, some researchers [21] suggested recently that these vacancies could exist at both A and B sites in PLZT.

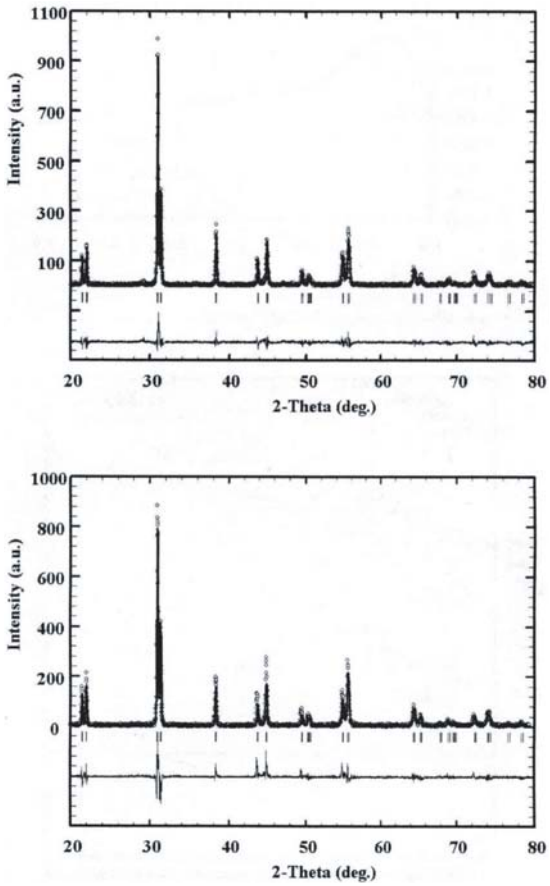

Fig. 2. Rietveld refinements of XRD patterns of (upper) PZT and (lower) PGZT ($x = 0.01$ % mole Gd^{3+}).

Table 1. Lattice parameters and tetragonality of PGZT.

% Mole	$a = b$	c	c/a
0.000	4.0338	4.1399	1.0263
0.010	4.0359	4.1374	1.0251
0.100	4.0313	4.1403	1.0271
0.500	4.0297	4.1423	1.0279
1.000	4.0279	4.1405	1.0279
2.000	4.0201	4.1290	1.0271
6.000	4.0224	4.1285	1.0264

3.2 ESR spectra

Each Gd-doped PZT powder samples were accurately weighed before putting it in the ESR sample tube so that the intensity of the Gd^{3+} ($4f^7$, electron spin $S = 7/2$, ^{155}Gd and ^{157}Gd both with nuclear spins $I = 3/2$) could be compared for different doping concentrations. The ESR spectra of powder specimens were measured by X-band ESR spectrometer at room (295 K) and liquid nitrogen (77 K) temperatures. The observed ESR spectra can be explained by the spin-Hamiltonian [22]

$$\boldsymbol{H} = \beta \boldsymbol{S} \cdot \boldsymbol{g} \cdot \boldsymbol{B} + \boldsymbol{D} \left[S_z^2 - S(S+1)/3 \right] + \boldsymbol{E} \left(S_x^2 - S_y^2 \right) + \boldsymbol{S} \cdot \boldsymbol{A} \cdot \boldsymbol{I}.$$

Here, the first term is Zeeman effect while β, $\boldsymbol{g}$, $\boldsymbol{B}$ and $\boldsymbol{A}$ are the Bohr magneton, gyromagnetic tensor, magnetic

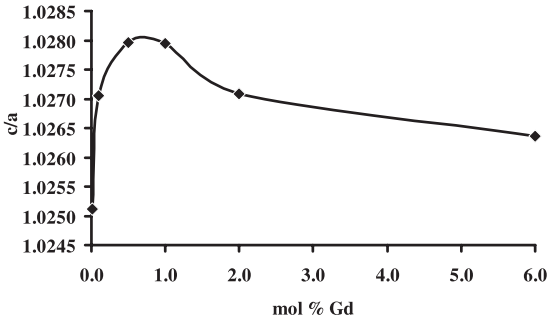

Fig. 3. Tetragonality of PGZT.

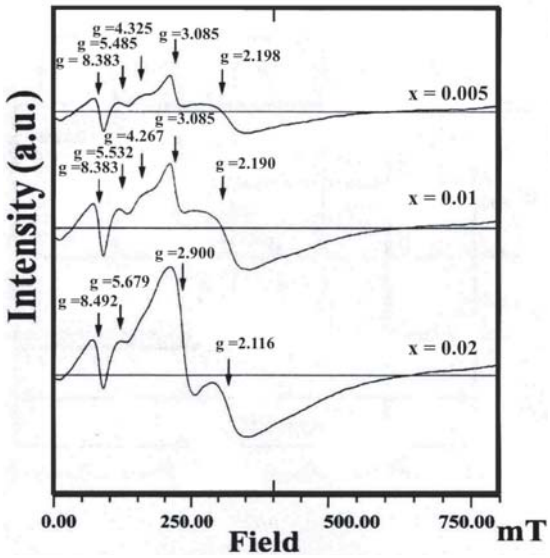

Fig. 4. ESR spectra of PGZT's at 295 K at microwave frequency 9.45 GHz.

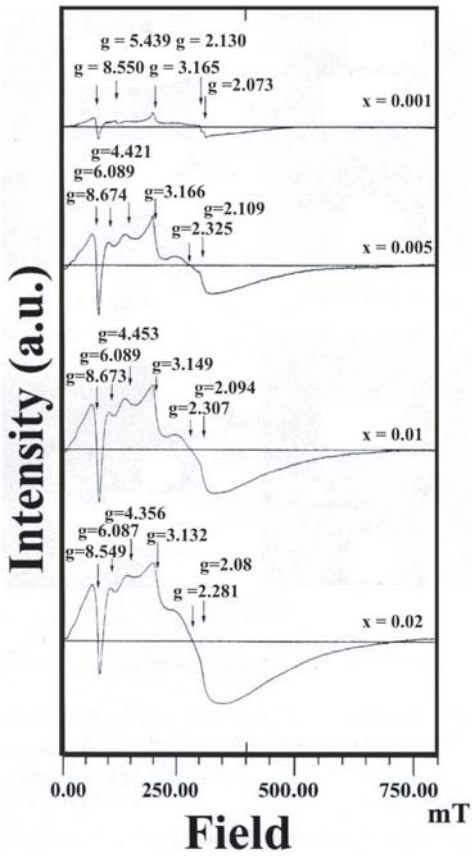

Fig. 5. ESR spectra of PGZT's at 77 K at microwave frequency 9.45 GHz.

field and hyperfine coupling tensor respectively. D and E are axial and rhombic crystal field parameters. The fine structure terms $D\ [S_z^2 - S(S+1)/3]$ and $E(S_x^2 - S_y^2)$ yield the major part of crystal field information. Two sets of powder ESR spectra of PGZT's are shown in Figures 4 and 5, corresponding to the spectra at 295 K and 77 K respectively. At 77 K, Gd^{3+} ($4f^7$) ions give a lot sharper signals than those at room temperature. There are essentially two sets of ESR signals. The first set shows some fine structure having one strong absorption peaks centered at 76.26 mT ($g = 8.550$), which corresponds to those Gd^{3+} ions at A sites. The second set is a seven-peak spectrum centered at 206.01 mT ($g = 3.165$), which belongs to the Gd^{3+} ions at B sites. This indicates that Gd^{3+} is in a tetragonal crystal field. It is clear that Gd^{3+} ions enter both A and B sites instead of only A site as has been widely believed. The shift in ESR signals clearly arises from the decrease in tetragonality as more Gd^{3+} ions enter A sites. Furthermore, the overlapped ESR strong absorption peaks from 0 to 300 mT ($g = 2.282-2.109$) belong to Gd^{3+} in unreacted Gd_2O_3. The existence of unreacted precursors is of minute amount, probably less than one percent and does not show clear XRD peaks. The ESR spectroscopy is a lot more sensitive in such a case. As a result, the intensity increases roughly linearly with respect to Gd^{3+} concentration. Furthermore, it is interesting to note that the ESR spectra indicate that all PGZT samples still in the tetragonality phase at 77 K. As can be seen, the increase of Gd^{3+} content from 0.05 to 2.00 mol % results in a gradual increase in the intensity of ESR absorptions in two different regions of the resonant magnetic field. This indicates that the some Pb^{2+} ions at A site are substituted by Gd^{3+} ions. As mentioned above, the ESR absorptions of Gd^{3+} ions appear in two areas at 206.01 mT ($g = 3.165$) and 0 to 300 mT ($g = 2.282-2.109$). The first band arises from Gd^{3+} ions at A site respectively while due to the site symmetry. Two sets resonant peaks at $g = 3.1650$ and $g = 2.282-2.109$ are from octahedral symmetry and tetragonal sites respectively. The second set of peaks arises from sites with weaker crystal field terms. Not only that, an earlier report on similar systems indicates that the result of this broad absorption may be due to the presence of O^{2-} random system [23,24]. To prove the point, the computer-simulated Gd^{3+} ions ESR signals from PGZT at room temperature and liquid nitrogen temperature (77 K) are given in Figures 6a and 6b, thus furnishing confidence in the spin-Hamiltonian parameters employed. The resulting best-fit values of g factor, $\boldsymbol{A}$, D and E parameters obtained, are $g_x = g_y = 5.851$ and $g_z = 8.550$, $A_x = 61.00$ G, $A_x = 65.50$, $A_z = 70.00$, $D = 55.00$ and $E = 8.00$ G, for Gd^{3+} at B site for $x = 0.005$ and for other concentrations of Gd^{3+} are listed in Table 2a. These values are different from those found for Gd^{3+} replacing Pb^{2+}at A site in

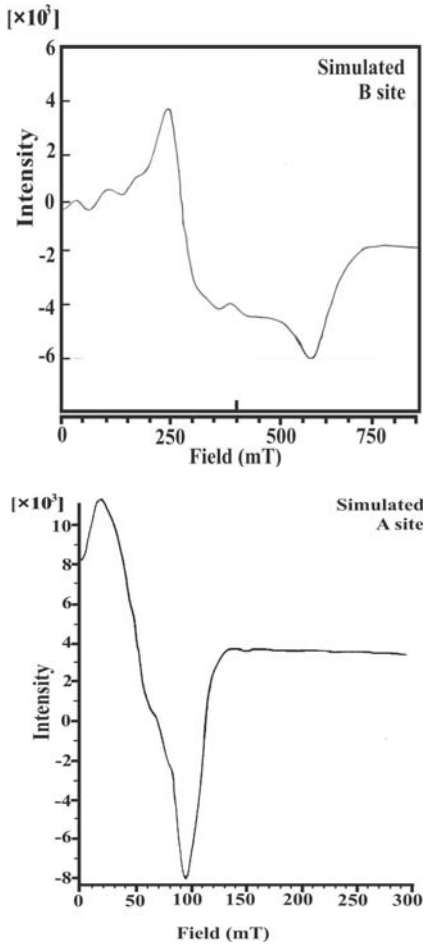

Fig. 6. Simulated ESR spectra at 77 K of PGZT for $x = 0.05$ % mole Gd^{3+} at (a) B site with ESR parameters $g_x = g_y = 4.582$, $g_z = 8.552$, $\boldsymbol{A}_x = \boldsymbol{A}_y = 60.00$, $\boldsymbol{A}_z = 70.00$, $\boldsymbol{D} = 55.00$ and $\boldsymbol{E} = 8.00$ Gauss, respectively, and (b) A site ESR with ESR parameters $g_x = g_y = 6.020$, $g_z = 8.134$, $\boldsymbol{A}_x = \boldsymbol{A}_y = 29.00$, $\boldsymbol{A}_z = 49.00$, $\boldsymbol{D} = 47.00$ and $\boldsymbol{E} = 20.00$ Gauss, respectively.

PGZT listed in Table 2b. The effects of Gd doping on the crystal field and piezoelectric properties of PGZT samples have been investigated further by varying gadolinium concentration. In order to carry out ESR quantitative analysis of the paramagnetic Gd^{3+} ions in the PGZT system, we have to estimate the number of resonators per gram (isolated Gd^{3+} ions in PGZT lattice).

3.3 Physical properties

Physical properties, namely, weight loss, volume shrinkage and density of PGZT sintered at 1200 °C for 1h are shown in Table 3. The percentage of weight loss after sintering increased significantly with increasing Gd concentration, which arises from PbO vaporization and subsequently, the creation of vacancies naturally to maintain charge balance. On the other hand, the volume shrinkage increased slightly, depending on the Gd content, which was due to denser grain formations. From the variation in sintering density with the percentage of Gd, it could be noticed that the density decreased significantly with Gd concentrations from 0.0 to 1.0 mol %, then the density increased slightly to about 7.8 g/cm^3 at 2.0 mol % Gd before going down slightly by 0.2 g/cm^3 from 7.8 to 7.6 g/cm^3. These results agree well with the theoretical density. The density decrease was related to the PbO loss. Furthermore, the oxygen vacancies were the slowest moving species and control the rate of densification in the PZT. As the Gd^{3+} ionic radius is relatively close to Pb^{2+}, Zr^{4+} and Ti^{4+}. Therefore, it seemed that Gd^{3+} probably went to both A (Pb^{2+}) and B (Zr^{4+} and Ti^{4+}) sites in the perovskite PZT system. The charge compensation would occur by creation of vacancies at A site and could be also by the decrease in the number of oxygen vacancies present in PZT system due to PbO evaporation. Therefore, the increasing of Gd content led to the decrease oxygen vacancies, which enhanced densification rate. Further indication, the density decreasing at about 2.0 mol % could as well be attributed to the reason that Gd^{3+} has reached its solid solubility limit in PZT solid solution.

Table 2a. ESR parameters at 77 K of Gd^{3+} in PGZT at B site.

Mole % (x)	$\boldsymbol{A}_x = \boldsymbol{A}_y$ (Gauss)	$\boldsymbol{A}_z$ (Gauss)	$g_x = g_y$	g_z	$\boldsymbol{D}$ (Gauss)	$\boldsymbol{E}$ (Gauss)
0.001	60.00	70.00	4.852	8.552	55.00	8.00
0.005	60.00	71.00	4.771	8.552	57.00	15.00
0.010	55.00	74.50	4.852	8.850	59.00	15.00
0.020	50.00	51.00	4.811	7.560	54.00	21.00

Table 2b. ESR parameters at 77 K of Gd^{3+} in PGZT at A site.

Mole % (x)	$\boldsymbol{A}_x = \boldsymbol{A}_y$ (Gauss)	$\boldsymbol{A}_z$ (Gauss)	$g_x = g_y$	g_z	$\boldsymbol{D}$ (Gauss)	$\boldsymbol{E}$ (Gauss)
0.001	29.00	49.00	6.020	8.134	47.00	20.00
0.005	39.50	60.00	6.892	8.634	45.00	21.00
0.010	38.00	59.00	6.920	7.034	45.00	19.00
0.020	25.50	45.00	6.892	8.634	48.00	20.00

Table 3. Physical properties of PGZT at various Gd^{3+} concentrations.

Mole % Gd	Weight loss (%)	Volume shrinkage (%)	Theoretical Density (g/cm^3)	Density (g/cm^3)	% Density
0.00	2.54	27.91	8.0827	7.7862	96.3317
0.01	3.63	32.82	8.1152	7.7496	95.4948
0.10	2.77	29.90	8.1005	7.7012	95.0707
0.50	3.60	33.69	8.1015	7.6852	94.8614
1.00	3.07	34.84	8.0873	7.6897	95.0836
2.00	5.00	32.01	8.1462	7.8080	95.8484
6.00	6.28	35.29	8.0866	7.7379	95.6879
10.00	14.31	38.25	8.0313	7.5638	94.1790

3.4 Dielectric and piezoelectric properties

Dielectric (1 kHz, 300 kHz) and piezoelectric properties of PGZT samples at different Gd concentrations are shown in Table 4. Comparing with the undoped PZT, the dielectric constant (ε_r at 1 kHz) of PGZT decreased slowly and then increased rapidly to reach a maximum at 1151.72 at 2.00 mole % Gd. Further doping led to a low value of only

Table 4. Dielectric and piezoelectric properties of PGZT.

Mole % Gd	ε_r 300 kHz	ε_r 1 kHz	k_p	Q_m	*DF*
0.00	835.12	960.10	0.39(5)	254.90	0.004(6)
0.01	723.14	876.20	0.34(2)	355.49	0.004(7)
0.10	855.02	950.71	0.33(3)	227.08	0.007(9)
0.50	746.95	978.37	0.39(6)	92.08	0.016(6)
1.00	919.57	1077.59	0.34(1)	83.27	0.018(1)
2.00	988.29	1151.70	0.34(9)	87.99	0.016(7)
6.00	873.09	941.05	0.29(0)	74.09	0.017(9)
10.00	595.72	606.54	0.21(1)	41.93	0.019(8)

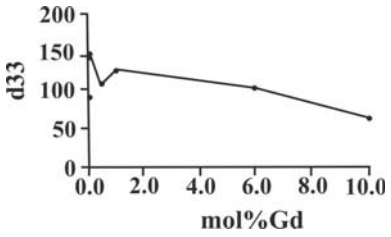

Fig. 7. Piezoelectric constant d_{33} of PGZT.

606.54 at 10 mole percent Gd which is considered overdoping here. This would be an adverse effect for PGZT in certain applications. Sharma [10] and Shannigrahi [25] reported similar effects on dielectric constant but with higher pyroelectric coefficients for gadolinium modified PZT (Zr:Ti = 60:40). The PGZT (60:40) could possibly be used as a pyrodetector up to T_c (125 °C). Furthermore, the dielectric constant tended to decrease as Gd^{3+} increased which was also found to be true in the present work. On the other hand, the value of electromechanical coupling coefficient, k_p was greatly enhanced for low concentrations up to 2.00 mole % Gd. Then it increased drastically to 0.29 and 0.21 at 6 mole % and 10.00 mole % Gd, respectively. The variation of the electromechanical quality factor, Q_m, as the function of Gd content in PZT (52:48) samples, is shown in Table 4. In this case, Q_m first increased sharply to 355.5 at 0.01 mole % Gd then decreased significantly to approximately 41.9 at 10 mole % Gd. On the other hand, the dissipation factor DF increased sharply from 0.005 for undoped to 0.019 at 10 mole % Gd sample as displayed in Table 4. The Gd doping into PZT had a dramatic effect on the piezoelectric constant d_{33} as it was only 91.00 pC/N for the undoped sample. It shot up and reached the highest value of 160 pC/N at 0.01 mole % Gd. Further doping proved detrimental as it depressed d_{33} to only 60 pC/N at 10 mole % Gd as shown in Figure 7.

4 Conclusion

It is evident that the Gd^{3+} doping into PZT should be no more than 2 mole % which is the solubility limit of the rare earth. This is also where the maximum dielectric constant (1 kHz) is reached. However, the optimal doping should be at 0.01 mole % Gd at which composition yield the best piezoelectric properties. XRD patterns show that PGZT samples still remain in tetragonal phase for $0.00 \leq x \leq 0.10$. Both tetragonality (c/a) and simulated ESR spectra indicate that Gd^{3+} ions can enter both A and B sites of the perovskite structure [26].

We wish to thank for the financial support from The Postgraduate Education and Research Program in Chemistry, Mahidol University to make this research possible.

References

1. B. Jaffe, W.R. Cook, H. Jaffe, Piezoelectric Ceramics (Academic Press, New York, 1971)
2. B. Noheda, D.E. Cox, G. Shirane, J.A. Gonzalo, L.E. Cross, S.-E. Park, Appl. Phys. Lett. **74**, 2059 (1999)
3. B. Noheda, J.A. Gonzalo, L.E. Cross, R. Guo, S.-E. Park, D.E. Cox, G. Shirane, Phys. Rev. B **61**, 8687 (2000)
4. R. Guo, L.E. Cross, S.-E. Park, B. Noheda, D.E. Cox, G. Shirane, Phys. Rev. Lett. **84**, 5423 (2000)
5. L. Bellaiche, A. Garcia, D. Vaderbilt, Phys. Rev. Lett. **84**, 5427 (2000)
6. F. Kulscar, J. Am. Ceram. Soc. **42**, 49 (1959)
7. T.K. Kamiya, T. Suzuki, T. Tsurumi, Jpn J. Applied Phys. **31**, 3058 (1992)
8. S. Takahashi, S. Hirose, Jpn J. Applied Phys. **31**, 3057 (1992)
9. H.D. Sharma, A.K. Tripathi, V. Chariar, T.C. Goel, P.K.C. Pilai, Mater. Sci. Eng. B **25**, 29 (1994)
10. G.H. Haertling, in *Electronic Ceramics*, edited by L.M. Levinson (Marcel Dekker, New York, 1988), pp. 371–492.
11. T.C. Goel, P.K.C. Pillai, H.D. Sharma, A.K. Tipathi, A. Tripathi, C. Pramila, A. Govinder, IEEE Transactions: Ultrasonic Ferroelectrics and Frequency Control **94**, 720 (1994)
12. R.C. Turner, P.A. Fuierer, R.E. Newnham, T.R. Shrout, Appl. Acoust. **41**, 299 (1994)
13. W.R. Cook, J.R. Jaffe, H. Jaffe, *Piezoelectric Ceramics* (New York, Academic Press, 1971)
14. J.S. Kim, K.H. Yoon, B.H. Choi, J.O. Park, J. Korean. Ceram. Soc. **27**, 187 (1990)
15. T. Kamiya, T. Suzuki, T. Tsurumi, M. Daimon, Jpn J. Appl. Phys. **31**, 3058 (1992)
16. K. Hayashi, A. Ando, Y. Hamaji, Y. Sakabe, Jpn J. Appl. Phys. **37**, 5237 (1998)
17. J.S. Kim, S.J. Kim, H.G. Kim, D.C. Lee, K. Uchino, Jpn J. Appl. Phys. **38**, 1433 (1999)
18. G. Galassi, J. Eur. Ceram. Soc. **19**, 1237 (1999)
19. H. Park, C.Y. Park, Y.S. Hong, K. Kim, S.K. Kim, J. Am. Ceram. Soc. **82**, 94 (1999)
20. J.A. Dean, Lange's Handbook of Chemistry, 13th edn. (McGraw Hill, New York, 1985)
21. K.H. Härdtl, D. Hennings, J. Am. Ceram. Soc. **55**(5), 20 (1972)
22. A. Abragam, B. Bleaney, *Electron Paramagnetic Resonance of Transition Irons* (Oxford, London, UK, Clarendon Press, 1970)
23. S. Boonyuen, L. Pdungsap, P. Winotai, T. Sudyodsuk, P. Petchpong, Int. J. Mode. Phys. B **16**(23), 3515 (2002)
24. P. Winotai, N. Udomkan, S. Meejoo, Sensor. Actua. A **122**, 257 (2005)
25. S.R. Shannigrahi, R.N.P. Choudhary, Mater. Res. Bull. **34**, 1875 (1999)
26. S.K.S. Parashar, R.N.P. Choudhary, B.S. Murty, Mater. Sci. Eng. B **110**, 58 (2004)